Nuclear Instruments and Methods in Physics Research A 368 (1996) 265–272

NUCLEAR INSTRUMENTS & METHODS IN PHYSICS RESEARCH Section A

Studies on the neutron field behind shielding of proton accelerators Part I: Concrete shielding

H. Dinter[a,*], K. Tesch[a], D. Dworak[b]

[a]*Deutsches Elektronen-Synchrotron DESY, Notkestr. 85, 22603 Hamburg, Germany*
[b]*Institute of Nuclear Physics, ul. Radzikowskiego 152, 31-342 Krakow, Poland*

Received 22 June 1995

Abstract

Energy- and angular distributions of neutrons behind concrete side shielding of proton accelerators were calculated. Simple arguments are given to understand the characteristic shape of the neutron spectrum. Calculations were repeated to receive data for simple shielding estimations. The dose equivalent attenuation coefficient of concrete for monoenergetic neutrons with energies between 1 and 400 MeV were determined and compared with the coefficient for neutrons leaving an accelerator shield at angles around 90°. Data for shielding gaps in accelerator shielding walls are given as an application. The calculations were performed by using the Monte Carlo codes FLUKA92 and MORSE.

1. Introduction

The highest contribution to the total dose equivalent behind a practical concrete side shield of proton accelerators is due to neutrons. A large amount of information on this neutron field was collected theoretically and experimentally in the last 5 years. For the calculations Monte Carlo codes have proved to be especially useful. A widely used program is the FLUKA code which was developed at CERN. It was used and extended in order to be able to calculate the complete neutron spectrum [1]. Since then the code was permanently improved and compared with measurements at CERN [2] and in Milan [3]. In the present paper we use the version FLUKA92 [4] together with a data library from ENEA [5] for neutrons below 20 MeV. In parallel to this development numerous measurements of the total neutron spectrum behind shields were performed at DESY and at CERN. Moderating Bonner spheres were used together with fission fragment counters for extension in energy range. The DESY instruments are described in Ref. [6].

Our knowledge of the neutron spectrum is detailed enough to calculate the most important magnitude, the total neutron dose equivalent H, and has important consequences for dose measuring techniques. Nevertheless some questions remain open. A qualitative understanding of the physical processes resulting in the characteristic shape of the neutron spectrum would be welcome. An important parameter for shielding calculations is the dose equivalent attenuation coefficient λ_H, in most cases given for side shielding. This coefficient should correspond to the λ_H for monoenergetic neutrons of those energies which dominate the high energy part of the spectrum.

Therefore we will first give examples of calculated and measured neutron spectra and of angular distributions together with arguments which explain the general shape of the spectra. Then the results of calculating the dose equivalent attenuation coefficients for monoenergetic neutrons between 1 and 400 MeV are presented. Finally we describe calculations to determine the dose attenuation of neutrons escaping the side shielding of proton accelerators, the results are compared with the results obtained for monoenergetic neutrons and with the conventional simple shielding formula. Data for shielding of gaps in shielding walls are derived from the calculations as a practical application.

2. Energy- and angular distributions of neutrons

In order to demonstrate the distribution of neutrons in energy and angle by a few examples we give some results of calculations for our "standard" shielding geometry (Fig. 1). Neutron fluence and dose equivalent depend on target thickness, thickness of concrete shield and position of detector, but the angle-integrated energy distribution (spectrum) is independent of the shield thickness as seen in Fig. 2 (primary energy 100 GeV, target diameter 10 cm,

* Corresponding author.

SSDI 0168-9002(95)00695-8

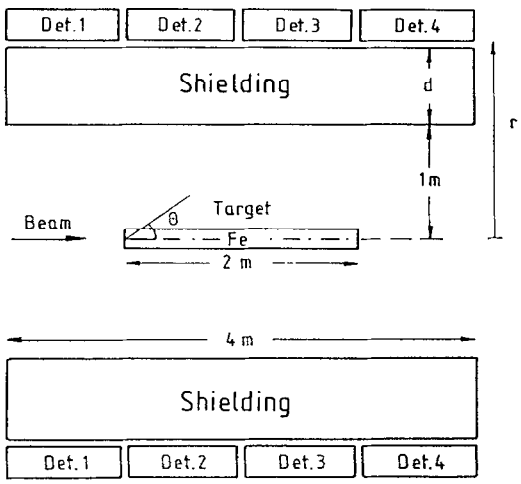

Fig. 1. Cylindrical shielding geometry.

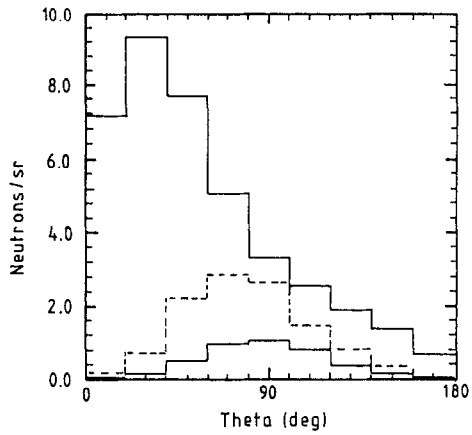

Fig. 3. Angular distribution of neutrons above 15 MeV per steradian and per one 100 GeV proton. Upper curve: neutrons escaping an iron target (10 cm ∅), broken line and lower curve: neutrons behind 80 or 160 cm concrete. Detectors 2 + 3 (see Fig. 1).

detectors 2 + 3; see Fig. 1). A linear–logarithmic plot is used in a way that the area under the curve between two energies is proportional to the fluence in that interval. Two distinct peaks show up; one is around 2 MeV, and neutrons above 15 MeV form a second peak and have a mean energy between 80 and 90 MeV. Angular distributions of the latter are displayed in Fig. 3. The expected forward distribution of neutrons leaving the iron target is shaped by the concrete side shielding so that a distribution peaked around 90° occurs behind a shield of practical thickness. A small change of the spectrum as a function of angle can be seen in Fig. 4, neutrons emerging from the 80 cm concrete shield at small angles have higher contribution of neutrons between 200 and 300 MeV. The shape of the neutron spectrum proved to be independent of the energy of the primary protons for proton energies above 5 GeV and to be nearly independent of the target thickness (except for a thick beam absorber). More details (such as selection of estimators for scoring current or fluence, appropriate fluence-to-dose conversion factors, position of detectors) can be found in Ref. [7].

The characteristic shape of the neutron spectrum behind concrete shielding with the two peaks at 2 and 100 MeV is also found by Gorbatkov and Kryuchkov [8] using another calculational method (one-dimensional discrete-ordinate method for solving the transport equation), different data base and different geometry.

The essential features of the spectrum were also verified by measurements. An example is shown in Fig. 5 which we measured at CERN with a 120 GeV proton beam hitting a copper target; the experimental facility is described by Hoefert and Stevenson [9]. Similar results we received at DESY. More than 30 spectra were taken behind existing shielding of concrete or concrete/sand combinations at the 7 GeV proton synchrotron. The source of stray radiation was the usual beam loss along the accelerator. This similarity of spectra confirms the independency of primary

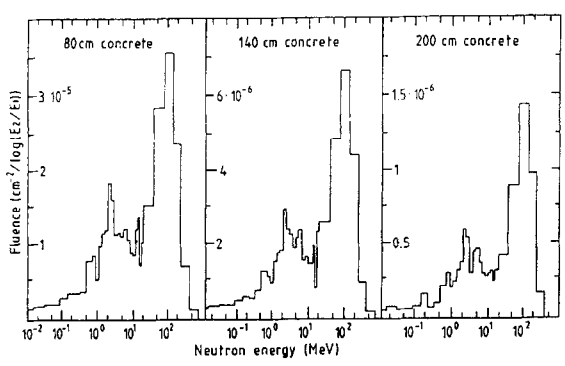

Fig. 2. Neutron spectra (fluence per logarithmic energy interval and per one 100 GeV proton) behind concrete shields of three thicknesses.

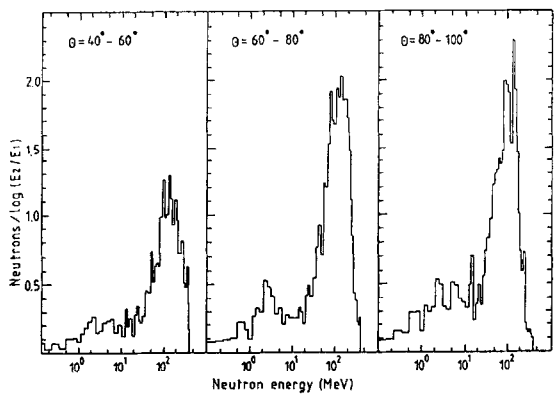

Fig. 4. Neutron spectra (number of neutrons per one 100 GeV proton) in three angular intervals behind 80 cm concrete.

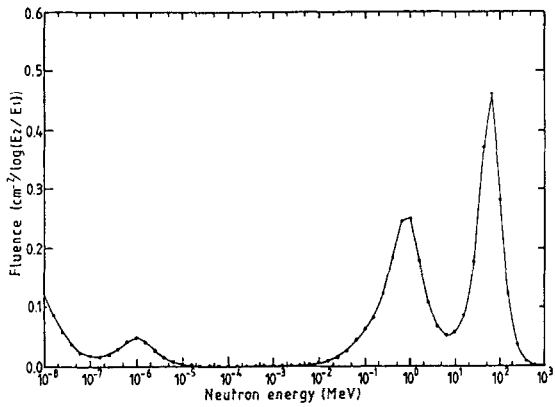

Fig. 5. Measured neutron spectrum (fluence per 2×10^4 protons of 120 GeV) behind 80 cm concrete.

energy, target, angle, and shield thickness. However, a closer inspection shows differences between calculations and measurements. The two peaks shown on a logarithmic energy scale are slightly shifted to lower energies in the experimentally determined spectrum. A similar effect is mentioned in Ref. [9]. It might be attributed to a shortcoming of the computational technique to unfold the spectrum from the measurements.

Simple qualitative arguments can be given that the described shape of the neutron spectrum may be anticipated. First we consider the high energy part above 15 MeV. This part is a rather flat distribution up to 100 MeV on a linear energy scale with a tail decreasing between 100 and 200 MeV; it shows up as a "peak" in Fig. 4 or 5 due to the compression on the usual logarithmic energy scale. These neutrons are the products of scattering of an incoming particle by the quasifree nucleons of complex nucleons, described as an intranuclear cascade, resulting in reactions of the type (p, xp yn). Cross sections of these reactions and especially energy distributions of neutrons and protons emitted at large angles are sparse. As an example we present some recently measured energy distributions of particles of (p, xn) and (p, xp) reactions in Fig. 6, left scale [10,11]. Other energy distributions of secondary particles for primary energies between 240 and 1840 MeV can be found in the papers of Bertini [11] and are of similar shape with the characteristic increase in intensity in the energy range from 100 or 200 MeV to 20 MeV. This increase of the products of the intranuclear cascade emitted at large angles is further modified by inelastic events in the thick target and/or the side shielding. Nonelastic neutron cross sections of nuclei are compiled and calculated by Alsmiller et al. [12], they are inserted into Fig. 6 for 3 nuclei (right scale). These cross sections are large enough to reduce effectively the produced cascade neutrons below 50 MeV either in a thick target or in a side shield. Fig. 7 shows examples which we calculated for both cases: the steep decrease of energy

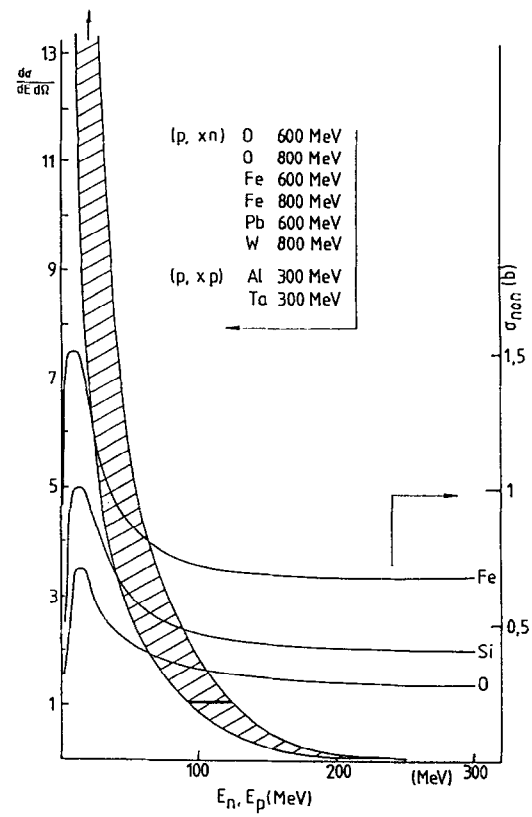

Fig. 6. Left scale: measured differential cross section of eight reactions at 90°, target nuclei and primary energies are given in the insert; the cross sections lie in the hatched area when normalized to unity between 100 and 120 MeV. Right scale: Nonelastic neutron cross sections for three nuclei.

distribution of neutrons leaving a target at 90° is reduced to a flat shoulder if the neutrons escape the thick target at small angles with a longer path in the target or if neutrons cross an 80 cm concrete side shield. And if this distribution is displayed on a logarithmic energy scale a peak around 100 MeV will show up. Loosely speaking: the right side of this peak is shaped by the intranuclear cascade, the left side is shaped by the extranuclear cascade. The physics responsible for the neutron spectrum behind a shield are interactions below 500 MeV; the high energy part (>500 MeV) of FLUKA or of any other code and its complexity or degree of perfection has no influence on calculated neutron spectra. This is also confirmed by the results of the next section.

The other peak around 1 MeV in any calculated or measured neutron spectrum is simple to identify. It is well known that after development of an intranuclear cascade initiated by a high energy particle the nucleus is left in an excited state and emits nucleons and especially neutrons called "evaporation neutrons" with a Maxwellian energy distribution.

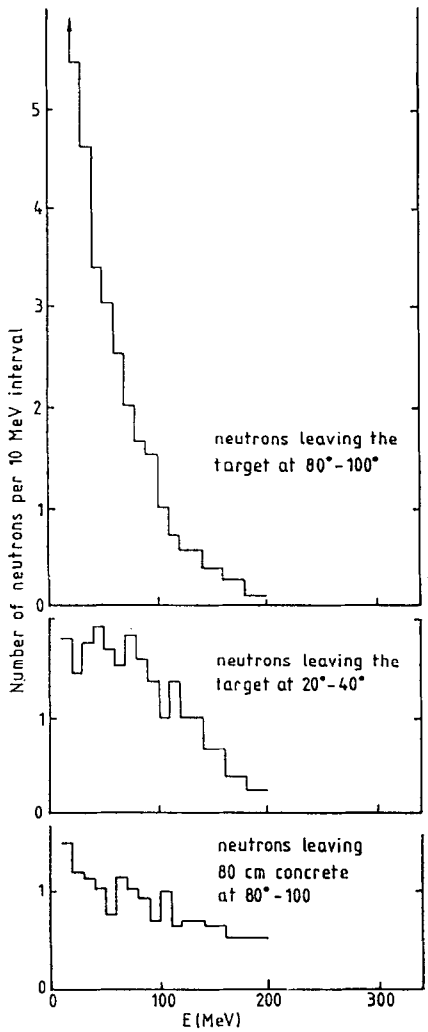

Fig. 7. Spectra of neutrons produced in an iron target (10 cm diameter) by 100 GeV protons plotted on linear scales.

3. Dose attenuation of monoenergetic neutrons

Experimental and theoretical results described in the preceding section show that the main contribution of high energy neutrons to the total dose equivalent behind side shielding is due to neutrons between 50 and 150 MeV. Therefore an important magnitude for shielding considerations is the dose equivalent attenuation coefficient in this range of neutron energies. These coefficients were first calculated by Alsmiller et al. [13] using the discrete ordinate code ANISN. Since these calculations (and calculations of other authors, see the compilation [14]) were performed 25 years ago we repeated them in order to have data of the same degree of reliability as other recent shielding calculations.

We applied the widely used Monte Carlo code MORSE (the actual version is from the HERMES code system [15]) and the HILO86 data library [12]. The same fluence-to-dose conversion factors were used as in our earlier papers [1], but the use of factors from ICRP21 give very similar attenuation coefficients. The geometry is a sequence of concrete slabs forming a cylinder. Behind each slab a "detector" is positioned with a diameter of 30 cm. A broad beam of monoenergetic neutrons hits the front face of the concrete cylinder (density 2.5 g/cm^3). The diameters of the neutron beam and the concrete are equal. The diameters depend on the primary neutron energy, they must be large enough so that the attenuation of neutron fluence is only due to interactions of neutrons with concrete nuclei and not due to neutrons escaping the system. One-way fluence was recorded by the detectors so that backscattered neutrons are not scored except by double-backscattering. The ratio of two-way fluence to one-way fluence was 1.7 at 1 MeV and 1.3 at 50 MeV primary neutron energy; recording one-way fluence or recording two-way fluence or use of a homogeneous concrete cylinder of variable length with only one detector behind gave the same attenuation coefficients.

The results are shown in Fig. 8 and in Table 1 where the energy group of the primary neutrons (according to the group structure of the used data library), the dimensions of the concrete cylinder, and the cut-off energy applied in the

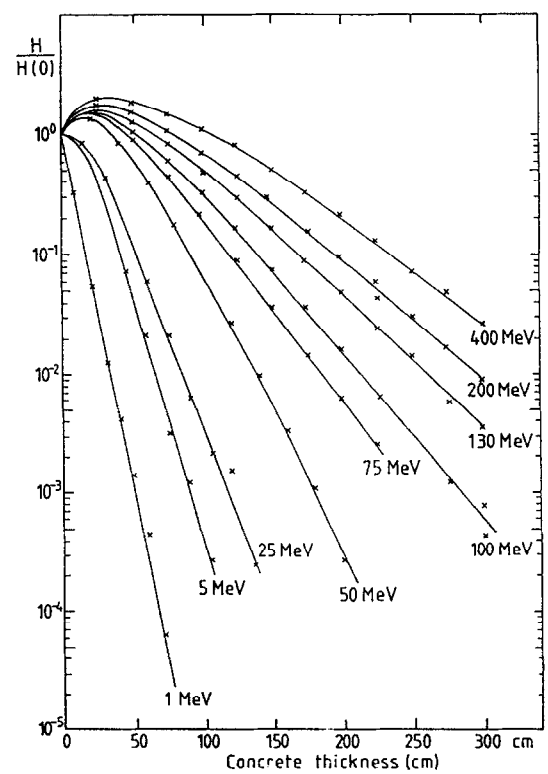

Fig. 8. Neutron dose equivalent in concrete for primary neutron energies between 1 and 400 MeV. The indicated primary energies are mean values of the corresponding energy groups (see Table 1).

Table 1
Data for calculating the neutron dose equivalent in concrete and the resulting attenuation coefficient λ_H

E_n [MeV]	Concr. cylinder		Cut-off energy [keV]	Range with expon. atten. [cm]	λ_H [g/cm^2]
	diam. [cm]	length [cm]			
0.91–1.1	120	70	0	0–70	18.7
4.5–5.5	120	120	0	30–105	27
22.5–25	150	150	0.15	30–135	36
45–50	180	200	15	100–200	50
70–80	180	225	15	75–200	72
90–100	300	300	15	100–300	79
120–140	300	300	15	100–300	99
180–200	300	300	15	100–300	112
375–400	300	300	15	125–300	129

calculations are listed. It cannot be expected that behind the buildup region the dose attenuation is purely exponential, but we assume an exponential decrease in that depth of the concrete cylinder which is indicated in Table 1 in order to derive an attenuation coefficient λ_H valid for a region of practical interest. The coefficients for the higher primary energies could possibly be somewhat smaller at a depth larger than 3 m because of the slight bending of the curves. The resulting attenuation coefficients are displayed in Fig. 9. Also entered are coefficients taken from the work of Alsmiller et al. [13] at the same ranges of thickness as in our work. It is remarkable that both calculations performed with completely different methods and data bases of different stages of development are essentially in agreement. Most recently we received a report of Kotegawa et al. [16] with results for the attenuation of monoenergetic neutrons received by using a modified HILO86 library. Their λ_H values valid for a concrete thickness of 300 cm are also added to Fig. 9.

The dose equivalent attenuation coefficient is not a well-defined magnitude due to its weak dependence on the material thickness, but Fig. 9 shows that information of sufficient reliability is available, especially with respect to its energy dependence for neutron energies expected behind accelerator concrete shielding.

We also calculated the neutron spectrum inside concrete for several energies of primary monoenergetic neutrons. The slab geometry described above would give spectra at 0° with respect to the incoming beam which is not interesting for side shielding problems. Therefore we changed the geometry: a one-dimensional neutron beam hits the center of the front face of a concrete hemisphere, its radius is 1.5 m. Spectra were taken at various angular intervals. Five examples are shown in Fig. 10 for primary energies of 100 to 400 MeV. The spectra show the same characteristic features as the spectra behind shielding of

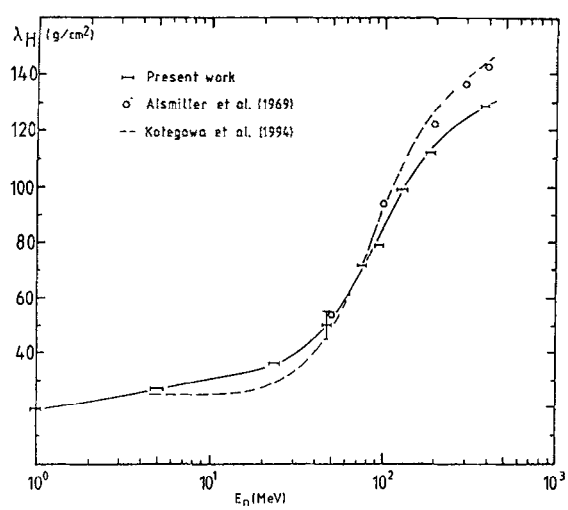

Fig. 9. Dose equivalent attenuation coefficient as a function of neutron energy (From Table 1).

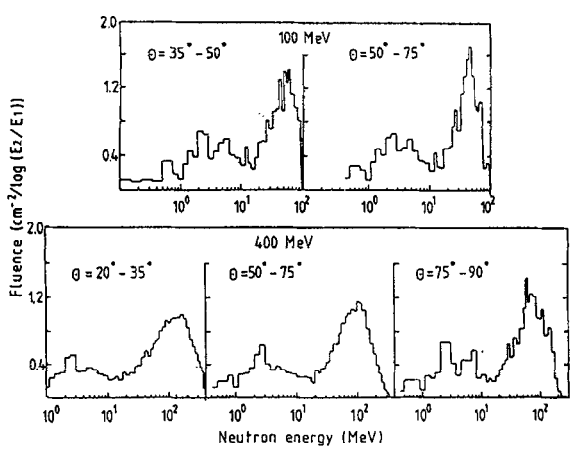

Fig. 10. Neutron spectra behind 150 cm concrete at several angular intervals with respect to a beam of neutrons with energy 100 or 400 MeV.

high energy accelerators, the two peaks of "cascade neutrons" and "evaporation neutrons". Also the slight shift of the high energy peak as a function of angle is seen. This similarity is expected from the qualitative arguments given in Section 2.

4. Dose attenuation coefficients of accelerator-produced neutrons

The most important parameter for shielding calculations is the dose equivalent attenuation coefficient λ of the neutron field behind accelerator shielding. Numerous experimental determinations were performed in the energy range 3 to 300 GeV and theoretical calculations for a geometry like that of Fig. 1. Results are usually fitted by a simple point-source formula of the type $H \sim \exp(-d/\lambda)/r^2$ where d and r are shield thickness and distance perpendicular to the beam respectively.

In connection with our calculations of neutron spectra mentioned in Section 2 we also calculated the total neutron dose equivalent H behind the shield in Fig. 1. The fluence-to-dose conversion factors of ICRP21 were used. Other details can be found in Ref. [7]. The results were fitted with

$$H = \frac{H_0}{r^2} E_p^{0.8} f_T e^{-d/\lambda'} . \quad (1)$$

We do not pretend that this equation in connection with Fig. 1 is a description of the physical phenomena of the shielding process, it is not more than a convenient parametrization of results which are important for dimensioning shields. The two parameters are $H_0 = 9 \times 10^{-15}$ Sv m^2 (if primary proton energy E_p is in GeV) and $\lambda' = 125$ g/cm^2. The coefficient f_T depends on the target thickness and is given in Table 2. The parameters are in agreement with earlier calculations [17] which give $H_0 = 6.9 \times 10^{-15}$ Sv m^2 and $\lambda' = 133$ g/cm^2; they were received by calculating "star densities" (number of inelastic interactions per unit volume) in the concrete shield and postulating a simple linear relationship between star density and neutron dose equivalent outside the shield. Experimental results were compiled and brought in the form of Eq. 1 in Ref. [18]; the resulting parameter H_0 is between 1×10^{-14} and 1.7×10^{-14} Sv m^2 and λ' is about 110 g/cm^2. The slight discrepancy between experimental and theoretical results is not astonishing, the experiments were performed at practical shielding and configurations which do not have the well-defined shielding geometry of Fig. 1.

Table 2
Target factor f_T for Eq. (1) for several target thicknesses (Fig. 1)

Diameter of target [cm]	f_T
10	1
5	0.85
2	0.67
0.2	0.28

In the following we will discuss the connection between the calculated parameter λ' of Eq. (1), the high energy part of the neutron spectrum described in Section 2, and the dose attenuation coefficient λ_H of monoenergetic neutrons (Section 3). Though such comparisons are not straightforward a check of consistency seems to be useful. The neutron spectra behind concrete side shielding show a peak around 100 MeV on a logarithmic energy scale (Fig. 2), or better: the main contribution of high energy neutrons to the total dose is due to neutrons between 20 and 150 MeV (the fluence-to-dose conversion factors are roughly constant in this region). For these neutrons a dose attenuation coefficient is expected which is below 100 g/cm^2, according to Fig. 9, whereas the calculated parameter λ' (see above) is about 130 g/cm^2. At first, the λ_H values of Fig. 9 are the dose attenuation coefficients of monoenergetic neutrons just behind the buildup region. They form the two characteristic peaks in the spectrum (Fig. 10) at larger angles to the incoming neutron beam. In contrary accelerator-produced neutrons show no buildup at all. Therefore such a comparison must be made with caution, nevertheless the discrepancy should be explainable. Eq. (1) together with Fig. 1 define an attenuation coefficient only for particles emitted perpendicular to the primary beam. This is the case for most of the neutrons behind side shielding, see Fig. 3, but not for all of them. Fig. 4 shows the slight dependence of the neutron spectra on angle, for angles $<90°$ there is an excess of neutrons with energies up to 300 MeV. Such a complicated field cannot be described in Eq. (1) or other point-source formulae, the λ' given above is a parameter important for practical shielding calculations but not an attenuation coefficient for any neutron group.

An attenuation coefficient in agreement with those coefficients calculated for monoenergetic neutrons can be expected for neutrons which emerge at angles around 90° with a spectrum like that of Fig. 4, right part; the mean energy of this spectrum is 80 MeV. In order to check this expectation we separated these neutrons from the cascade development in the shield. Neutrons produced in the target or emerging a concrete shield were allowed to stream through a gap in the shield (which acts as some kind of collimator) so that they dominate the dose behind the gap and their dose attenuation coefficient can be determined by means of additional slabs of concrete positioned behind the slit. The geometry is shown in Fig. 11.

The calculations were performed in two steps. First the plane source indicated in Fig. 11 was calculated by means of FLUKA92 code to receive a neutron distribution in energy and two angles. Second, neutrons with this distribution were emitted uniformly from this plane; their path through the block and the gap and through the additional concrete slabs behind the gap were calculated using the

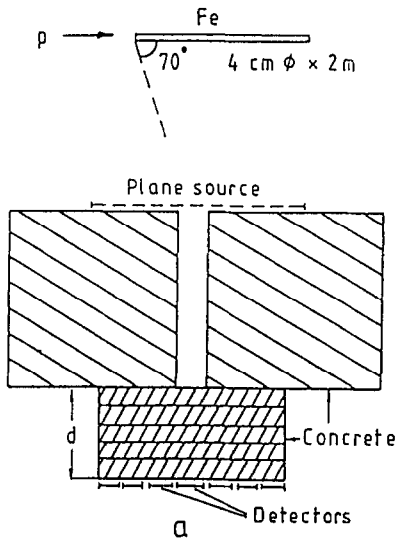

Fig. 11. Geometry for calculating the dose equivalent attenuation of neutrons streaming through gaps in shieldings.

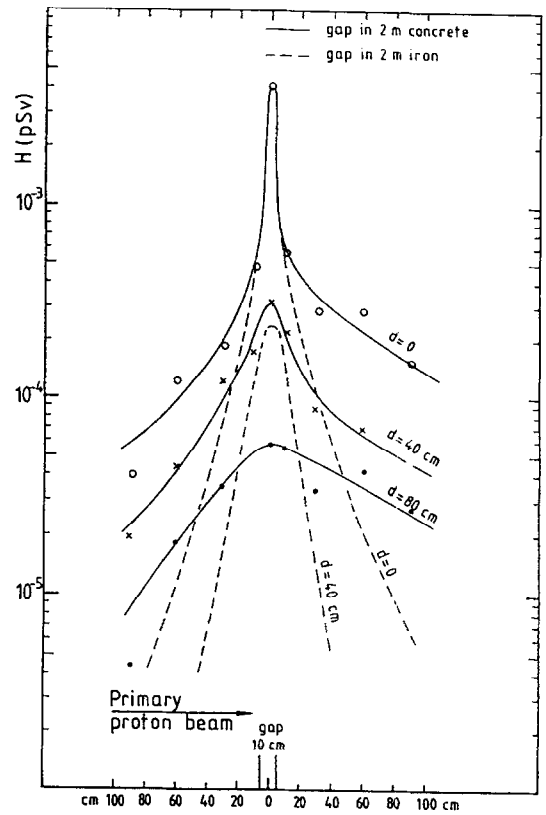

Fig. 12. Longitudinal distribution of the neutron dose equivalent per one 100 GeV proton behind a gap in a concrete or iron side shielding block (Fig. 11); d is the thickness of the concrete gap shielding.

MORSE code. The widths of the gap were 30, 10 or 3.3 cm. The one-way fluence scored in the "detectors" was converted to dose equivalent. The central detector always had the same dimensions as the cross section of the gap, the heights of gaps and detectors were 2 m. The neutron spectrum in the central detector just behind the gap shows a high contribution of evaporation neutrons produced in the gap (especially behind a gap in an iron block), but behind additional 20 to 40 cm concrete the spectrum calculated behind a gap of width 30 cm has the typical shape of a neutron spectrum behind bulk concrete shielding at 90°. Therefore we can study the attenuation behaviour of this component in a better defined geometry. The purely geometrical attenuation was eliminated by calculating the dose for the same geometry but without concrete in the shielding slabs. We found an exponential decrease for the dose equivalent behind all gaps when only neutrons above 12 MeV were considered and the same behaviour for all neutrons behind a minimum gap shielding of 20 cm concrete. The resulting attenuation coefficients are shown in Table 3, they scatter around 80 g/cm^2. This is the dose attenuation coefficient of monoenergetic neutrons of about 90 MeV according to Fig. 9. With such values the discrepancy mentioned above is solved. The dose attenuation coefficient calculated for neutrons leaving a concrete shield at angles around 90° and the high energy part of their spectrum is consistent with the corresponding attenuation coefficient calculated for monoenergetic neutrons.

5. An application: shielding of a gap

It happens that adjacent concrete blocks or shieldings of different materials form a gap which, e.g., is readily used

Table 3
Dose equivalent attenuation coefficient of neutrons streaming through gaps perpendicular to the primary beam. Second column: neutrons above 12 MeV. Third column: all neutrons, but gap shielding d larger than 20 cm

Geometry	λ(g/cm^2)	
	$E_n > 12$ MeV	All neutrons ($d > 20$ cm)
2 m concrete block, gap 30 cm	87	75
2 m concrete block, gap 10 cm	73	70
1 m iron block, gap 10 cm	78	≈77

as a duct for cables etc. This is the geometry of Fig. 11. It is clear that the necessary shielding of such a slit can be thinner than the basic shielding wall but quantitative information is not at hand up to now. We therefore calculated the neutron dose equivalent behind a minimum gap shielding of 20 cm as a function of the gap width g; the result is

$$H(20) = \frac{H_0}{r^2} E_p^{0.8} f_T g\,; \quad H_0 = 5 \times 10^{-17}\ \mathrm{Sv\,m^2}\,, \tag{2}$$

with g in cm, the other symbols having the same meaning and dimensions as in Eq. (1). The equation is valid for g in the range 3 to 30 cm. Further attenuation in concrete can be calculated by using the coefficient 80 g/cm^2. The amount of overlap can be estimated from Fig. 12 where the dose equivalent is calculated behind concrete or iron blocks with a gap of 10 cm width, the distribution is given perpendicular to the gap (i.e. parallel to the primary beam) behind concrete gap shielding of 40 or 80 cm.

References

[1] J.M. Zazula and K. Tesch, Nucl. Instr. and Meth. A 286 (1990) 279.

[2] A. Fassò, A. Ferrari, J. Ranft, P.R. Salla, G.R. Stevenson and J.M. Zazula, Nucl. Instr. and Meth. 332 (1993) 459.

[3] C. Birattari, E. de Ponti, A. Esposito, A. Ferrari, M. Pellicioni and M. Silari, Nucl. Instr. and Meth. A 338 (1994) 534.

[4] A. Fassò, A. Ferrari, J. Ranft, P.R. Salla, G.R. Stevenson and J.M. Zazula, Proc. Workshop on Simulating Accelerator Radiation Environment, Santa Fe, 1993.

[5] E. Cuccoli, A. Ferrari and G.C. Panini, JEF-DOC-340 (1991).

[6] H. Dinter and K. Tesch, Radiat. Prot. Dosimetry 42 (1992) 5.

[7] H. Dinter and K. Tesch, Internal Report DESY D3-78 (1994).

[8] D.V. Gorbatkov and V.P. Kryuchkov, IHEP Report 94-47, Protvino 1994; Part. Accel. Conf., London (1994).

[9] M. Höfert and G.R. Stevenson, 8th Int. Conf. on Radiation Shielding, Arlington, Texas (1994).

[10] W.B. Amian, R.C. Byrd, D.A. Clark, C.A. Goulding, M.M. Meier, G.L. Morgan and C.E. Moss, Nucl. Sci. Eng. 112 (1992) 78; 115 (1993) 1.

[11] H.W. Bertini, Phys. Rev. 131 (1963) 1801; 188 (1969) 1711; 2nd Int. Conf. Accel. Dosimetry, Stanford, 1969; Nucl. Phys. A 187 (1972) 531.

[12] R.G. Alsmiller, J.M. Barnes and J.D. Drischler, Nucl. Instr. and Meth. A 249 (1986) 455.

[13] R.G. Alsmiller, F.R. Mynats, J. Barish and W.W. Engle, Nucl. Instr. and Meth. 72 (1969) 213.

[14] R.H. Thomas and G.R. Stevenson, Radiological Safety Aspects of the Operation of Proton Accelerators, IAEA Technical Reports Series No. 283, Vienna (1988).

[15] P. Cloth, D. Filges, R.D. Neef, G. Sterzenbach, Ch. Reul, T.W. Armstrong, B.L. Colborn, B. Anders and H. Brückmann, Jül-2203, Jülich, Germany (1988).

[16] H. Kotegawa, S. Tanaka, Y. Sakomoto, Y. Nakane and H. Nakashima, Jpn. At. Energy Res. Inst., JAERI-Data/Code 94-003 (1994).

[17] Landolt-Börnstein, Numerical Data in Science and Technology, NS 11 (1990) p. 126.

[18] K. Tesch and H. Dinter, Radiat. Protection Dosimetry 15 (1986) 89.